Exploring the Human-Nipah virus protein-protein interactions

Luis Martinez-Gil[1,*], Natalia M. Vera-Velasco[1], Ismael Mingarro[1]

[1]Department of Biochemistry and Molecular Biology, ERI BioTecMed, University of Valencia, Dr. Moliner 50, 46100 Burjassot, Spain. luis.martinez-gil@uv.es.

[*]Corresponding author. Email: luis.martinez-gil@uv.es

Abstract

Nipah virus is an emerging, highly pathogenic, zoonotic virus of the paramyxoviridiae family. Human transmission occurs by close contact with infected animals, the consumption of contaminated food, or, occasionally, via other infected individuals. Currently, we lack therapeutic or prophylactic treatments for Nipah virus. To develop these agents we must now improve our understanding of the host-virus interactions that underpin a productive infection. This aim led us to perform the present work, in which we identified (101) human-Nipah virus protein-protein interactions (PPIs), most of which (88) are novel. This dataset provides a comprehensive view of the host complexes that are manipulated by viral proteins. Host targets include the PRP19 complex and the miRNA processing machinery. Furthermore, we explored the biologic consequences of the interaction with the PRP19 complex and found that the Nipah virus W protein is capable of altering p53 control and gene expression. We anticipate that these data will help in guiding the development of novel interventional strategies to counter this emerging viral threat.

Importance

Nipah virus is recently discovered virus that infects a wide range of mammals, including humans. Since

its discovery there have been yearly outbreaks and in some of them the mortality rate has reach 100% of the confirmed cases. However, the study of Nipah virus has been largely neglected and currently we lack treatments for this infection. To develop these agents we must now improve our understanding of the host-virus interactions that underpin a productive infection. In the present work we identified 101 human-Nipah virus protein-protein interactions using an affinity purification approach coupled with mass spectrometry. Additionally, we explored the cellular consequences of some of these interactions. Globally, this dataset offers a comprehensive and detailed view of the host machinery's contribution to the Nipah virus's life cycle. Furthermore, our data present a large number of putative drug targets that could be exploited for the treatment of this infection.

Introduction

Nipah virus is an emerging, highly pathogenic, zoonotic virus from the paramyxoviridiae family (1, 2). The virus was first detected in humans in 1998, in Malaysia (3), and since then fatal cases have been reported yearly. The first outbreaks in Malaysia and Singapore were associated with severe febrile encephalitis with a case fatality rate of 38%. More recent outbreaks in Bangladesh and India are linked with respiratory disease and manifest an even higher case fatality rate, that occasionally reaches a staggering 100% (4). Transmission to humans occurs mostly by close contact with infected animals or by consuming contaminated food (5). However, incidents of human-to-human transmission have also been reported (6), with these being the major route of infection for the Bangladeshi strains (7). Currently, there are neither therapeutic nor prophylactic treatments for Nipah virus. Despite the low number of annual cases, the virus's broad host range and increased pathogenesis warrants attention given the major health threat that this virus could pose. However, disappointingly, the study of Nipah virus has been largely neglected.

47

48 The Nipah virus comprises a 6-gene, 18.2 Kb, negative ssRNA genome, which encodes 9 proteins:
49 Nucleoprotein (N), Phosphoprotein (P), the interferon antagonists W and V, the viral C protein, a
50 matrix protein (M), viral fusion and glycoproteins (F and G, respectively), and a large polymerase (L).
51 Host attachment is achieved by the viral G protein that binds to the host cell surface receptors ephrin
52 B2 or B3 (8, 9). Next, the cellular and viral membranes fuse and the capsid disassembles to deliver the
53 viral genome into the cell. Once in the cytoplasm, the viral messenger and genomic RNAs are
54 synthesized and translated to generate viral proteins. Successful infection requires evasion of the
55 interferon (IFN)-α/β response (10, 11) (a key component of the innate immune response to virus
56 infection). Four Nipah-encoded proteins (P, V, W, and C, all encoded by the *P* gene) participate in
57 overcoming the innate immune response (12, 13). The generation of these proteins relies on varying the
58 reading frame, or using an alternate reading frame when transcribing *P*. In order to vary the reading
59 frame, the fidelity of transcription is interrupted. Specifically, the polymerase stutters at an AG patch of
60 sequence, which results in the insertion of supplementary G residues into the nascent mRNA. While the
61 unedited *P* mRNA encodes the P protein, insertion of one or two extra G residues shifts the frame to
62 produce the V and W proteins, respectively; the C protein is synthesized from an alternate open reading
63 frame (14). A large proportion of the P, V, and W protein sequences are identical (406 amino acids of
64 709, 456, and 449 amino acids, respectively) and, consequently, share some functions. All three
65 proteins inhibit the Jak-STAT signaling pathway by binding to STAT1 and preventing its
66 phosphorylation in response to IFN (15–18). In addition, the V protein inhibits MDA5 signaling (which
67 is conserved across paramyxoviruses) (19–21), while the W protein blocks Toll-like receptor (TLR) and
68 Rig-I-like receptor (RLR) signaling (downstream of IFN regulatory factor 3 activation) (22). The
69 different functions of the V and W proteins can be attributed to their sequence differences and distinct
70 sub-cellular localizations. While V is mostly cytosolic, W is conveyed to the nucleus by virtue of a

71 nuclear localization signal (NLS) at its unique carboxy terminus (Ct). In addition to the proteins
72 encoded by the *P* gene, the M proteins have also been reported to be involved in antagonizing the
73 innate immune system by targeting TRIM6, IKK, and unanchored polyubiquitin chains (23).
74
75 Identifying and understanding host-virus interactions are fundamental to our comprehension of the
76 mechanism of infection, and how this can be used to inform the development of vaccines or antivirals.
77 Previously, a variety of technologies have been used to identify host-virus protein-protein interactions
78 (PPIs). These include tandem-affinity purification (TAP) coupled with mass spectrometry (MS) (TAP-
79 MS) (24, 25), two-hybrid system screens (26), or protein-fragment complementation assays (27). The
80 TAP-MS approach, particularly for a biosafety level 4 (BSL4) pathogen, such as Nipah virus, offers
81 significant advantages. First, TAP-MS is a sensitive and unbiased method with which to identify PPIs.
82 Second, the expression, purification, and identification of PPIs for individual viral proteins constitutes a
83 risk-free and laboratory-friendly approach. Third, the resultant dataset should provide a comprehensive
84 analysis of the complexes that are formed, and the pathways that are triggered during the viral life
85 cycle. However, TAP-MS of non-cellular genes expressed from a plasmid driven system does not fully
86 recapitulate the viral context and might lead to an erroneous identification of PPI.
87
88 In the present work, we aimed to identify the human proteins associated with Nipah virus proteins
89 using a TAP-MS approach. We identified 101 PPIs, 88 of which were previously unreported. We
90 uncovered a number of host complexes targeted by the virus, including interactions with the PRP19
91 complex and miRNA processing machinery. Furthermore, we explored the biologic consequences of
92 these PPIs and found that the Nipah virus W protein is capable of altering p53 control and gene
93 expression. Globally, this dataset offers a comprehensive and detailed view of the host machinery's
94 contribution to the Nipah virus's life cycle. Furthermore, our data present a large number of putative

drug targets that could be exploited for the treatment of this life-threatening infection. Nonetheless, before drawing any conclusions on the functional relevance of any of these interactions results must be validated in a viral context**.**

Results

Purification, identification, and analyses of human-Nipah virus PPIs. To identify human proteins associated with Nipah virus we cloned the sequence of each known Nipah virus protein using a mammalian expression vector. Each protein was fused to a TAP tag (comprising 2xStrepII and 1xFlag) (28) at either its amino (Nt) or carboxy (Ct) terminus. Independent tags at either terminus were used to minimize the possibility of missing a PPI due to tag-masking. This strategy also allowed us to identify which protein end, if any, was prone to the interaction. Enhanced Yellow Fluorescent Protein (EYFP, *Aequorea victoria),* the Red Fluorescent Protein (RFP, *Discosoma sp*.), and an empty vector were included as negative controls. Clones were transfected into HEK-293T cells, with tagged proteins purified 48 hrs post transfection using, in tandem, the Streptavidin and Flag affinity labels. Final eluates were then analyzed by SDS–polyacrylamide gel electrophoresis for quality control, and by MS to identify interaction partners (Fig. 1a). After careful evaluation, the L protein derived samples were not submitted for MS analysis due to insufficient protein. Fusion of the C protein to EYFP was used to improve purification yields prior to PPI identification by MS. See materials and methods for a complete list of the constructs used and the number of replicates analyzed by MS. For each bait, only proteins identified in two or more replicates were considered to be potential interactors. Further, protein hits identified in any of the control experiments (using EYFP, RFP, or empty plasmid) were discarded. To further eliminate artifacts we compared our hits to those recorded in the CRAPome database (29), which lists affinity purification contaminants. Specifically, the experimentally obtained ratio for a

protein hit (i.e. the number of times a protein was identified with a particular bait/ replicate number (for that bait)) had to exceed that recorded in the CRAPome database by (at least) five fold. The abundance of the interaction was then estimated using the exponentially modified Protein Abundance Index (emPAI). To compare protein abundance across experiments, emPAIs for each protein were divided by the median emPAI value for the sample (emPAI/med). Since some hits were obtained in 2, 3, 4, or even in 5 replicates, to accurately evaluate their abundance, we calculated the average logarithm of the emPAI/med (ave log(emPAI/med)). As expected, the higher the number of times a protein was found, the higher its ave log value (emPAI/median; Fig. 1B, the unique PPI identified in 5 replicates is not represented in the bar graph). These data suggested a robust protein identification and selection protocol. A total of 101 PPIs were identified between human and Nipah virus proteins (Table 1) of which 88 were previously unreported. As we had placed the TAP tag at the N and C termini of the bait constructs we could analyze which position, if any, favored the detection of the interactor proteins. Overall, 64.4% of the interactors were identified irrespective of tag position, while 18.8% and 16.8% of the PPIs were identified, exclusively, when the affinity tag was either N- or C- terminal, respectively (Fig. 1C). For some Nipah virus proteins the tag position was irrelevant in terms of identifying partner proteins (e.g. for the P, V, and W proteins) (Fig. 1C). For other Nipah proteins (C, and in particular, G), the location of the affinity label greatly influenced the host protein-bait interaction. Interestingly, three of these proteins (F, G, and C) associate with cellular membranes. It is worth noting that, for proteins detected in two replicates, the ave log (emPAI/med) values were higher when identification was tag-position dependent (Fig. 1B).

Next, we analyzed the functional categories of host proteins associated with each Nipah virus bait. Based on the current literature, certain results were anticipated. These included an association of the F protein with the endoplasmic reticulum (30), and the G protein with the Ephrin receptor pathway (8).

142 The nuclear localization of W (18), the shuttling of protein C between the cytoplasm and nucleus (31),
143 and the association of M with the ubiquitin machinery (23, 32), were all consistent with previous data
144 (Figs. 1D and E). Conversely, some other highly enriched categories were unexpected. These included
145 an association of the PRP19 complex with the P, V, and W proteins, and the enrichment of RNAi
146 related proteins in the M-interactor list. Furthermore, a careful review of the literature revealed that
147 36.4% of the hits had previously been reported as viral protein interactors (Fig. 1F). When a random
148 list of 101 proteins was queried, only 8% were described as viral interactors (Fisher-test enrichment
149 Log2 p-value= -17.14). The identification of known functions of Nipah virus proteins using GO term
150 analyses, and the elevated percentage of hits previously associated with viral functions, greatly
151 increases our confidence in this dataset.
152
153 One of the main objectives of our work was to identify potential drug targets for the treatment of Nipah
154 virus. With this in mind, we searched for drugs that could target any of the proteins obtained in our
155 TAP-MS analyses. To this end we utilized the DRUGBANK database (a bioinformatics and
156 cheminformatics resource that combines drug data (i.e. chemical, pharmacological and pharmaceutical)
157 with comprehensive drug target information (i.e. sequence, structure, and pathway)) (33, 34). In our
158 search we identified 11 drugs (including FDA approved compounds) that could target the Nipah virus's
159 cellular interactors. These data are summarized in Table 2.
160
161 To visualize these host-virus interactions we plotted the 101 PPIs as a network schematic (Fig. 2), with
162 inclusion of the PPIs for cellular proteins derived from the IntACT (https://www.ebi.ac.uk/intact/) (35)
163 and String databases (http://string-db.org/) (36) (dotted lines, Fig. 2). Collectively, the network contains
164 93 nodes (corresponding to human and Nipah virus proteins) and 126 interactions (edges). Many of the
165 known PPIs (involving the viral G, F, M, W, and V proteins) were identified in our assays (denoted by

166 the double black lines) (8, 9, 21, 22, 32, 37–42) and support the quality of our approach. Surprisingly,
167 we also detected an interaction between the W protein and STAT4, although a previously reported
168 interaction with STAT1 went undetected (Shaw et al. (18)). To confirm the potentially new interaction,
169 we performed a pull-down experiment using V, W, V_{G121E}, and W_{G121E} protein lysates (the mutants
170 cannot bind STAT1 (43)) with the resolved proteins probed for STAT1 and STAT4 expression. EYFP
171 was included in the assay as a negative control. The experiments revealed strong interactions between
172 the wild type V and W proteins and both STATs 1 and 4 (Fig 3). Conversely, neither V_{G121E} nor W_{G121E}
173 bound either STAT.
174
175 **Interaction of the Nipah virus with the PRP19 complex.** The network map helped to identify robust
176 associations between the P, V, and W proteins and the PRP19 complex (Fig. 2 and Fig. 4A and B). The
177 PRP19 complex (also known as PRPF19 or the NeeTeen Complex (NTC)) participates in key cellular
178 processes (for a full review on PRP19 complex functions see (44)) that include splicing (45),
179 transcription elongation (46), and genome maintenance (47). Additionally, the PRP19 complex has
180 been identified as a negative regulator of p53 [48, 49]. First, we sought to validate the PRP19-viral PPI
181 identified in the TAP-MS experiments. Using the TAP tag, we pulled-down both the V and W proteins
182 (and EYFP) and then performed immuno-blots for select PRP19 complex constituents (namely
183 CDC5L, PRP19, PLRG1, and BCAS2; Fig. 4C). Mutants (G121E) of the Nipah virus V and W proteins
184 were also included in this assay. Subsequent results confirmed the TAP-MS data, with an association
185 between the viral proteins and the PRP19 complex detected, even in the presence of mutants deficient
186 in STAT1 binding (V_{G121E} and W_{G121E}).
187
188 The PRP19 complex manifests multiple activities in the nucleus. On the basis of Nuclear Localization
189 Signal (NLS) expression, only the Nipah virus W protein (of all the proteins encoded by the *P* gene) is

predicted to be able to access this compartment. A robust nuclear co-localization between PLRG1 tagged with Yellow Fluorescent Protein (YFP) and the W protein was detected (Fig. 4D). When the viral V or P proteins were co-expressed with YFP-PLRG1, only marginal co-localization at the peri-nuclear region could be detected (Fig. 4D, arrowheads). These results suggest that the strong interactions seen in the TAP-MS experiments between PRP19 and the V and P proteins might have occurred post lysis following disruption of the cellular nuclear envelope.

Next, we sought to discover whether the Nipah virus could interfere with the biologic functions of the PRP19 complex. First, we analyzed the activity of p53 in the presence of viral proteins. For this purpose we used a luciferase-based p53-activity reporter assay (50). Briefly, a reporter plasmid containing a p53 DNA-binding site upstream of a luciferase reporter was co-transfected with the protein of interest into HCT116 cells (a human-derived cell line that retains p53 activity); EYFP was used to normalize the data (white bar panel a). Interestingly, transfection and expression of the Nipah virus W **(**black bar, panels A, B and C) protein rendered higher luciferase values than EYFP (Fig. 5A). Conversely, transfections with P or V failed to alter p53 activity, as may be predicted from their cytosolic expression patterns and showed luciferase values significantly lower that those obtained with W. However, based on our TAP-MS data, both the Nipah virus V and P proteins are capable of interacting with the PRP19 complex if present in the same compartment/space (as occurred post lysis). When we altered the expression pattern of the V protein by supplementing its sequence with an NLS (V_{NLS}) (22) we observed an increase in p53-dependent luciferase expression. Conversely, elimination of the NLS in the W protein ($W_{BR34\ (22)}$) reduced p53 activity back down. In accordance with our pull-down assays, the elimination of STAT1 binding failed to influence the effects of the Nipah virus V or W proteins on luciferase expression (Fig. 5A).

214 To analyze the role of Nipah virus W protein on p53 activity in the presence of stress/apoptotic stimuli,
215 HCT116 cells were either treated with Doxorubicin (a known inducer of p53 activity (51)) or were
216 infected with Newcastle disease virus (NDV). NDV is a -ssRNA paramyxovirus with a genome
217 structure similar to Nipah (52), that has been used for functional studies of Nipah virus proteins (13).
218 Irrespective of the cellular stress (infection or apoptosis; Figs. 5B and C), the EYFP-associated values
219 were higher than those for the mock treated samples, confirming that p53 activity had been stimulated
220 by the selected stimuli. In the cell stress scenarios (including viral infection), the Nipah virus W protein
221 further enhanced p53 activity with nuclear localization of the W or V proteins key in achieving this
222 activation, as confirmed in A549 cells (Fig. 5 D-F).
223
224 Next, we decided to investigate the potential influence of the Nipah virus W protein on PRP19
225 complex-mediated gene expression and splicing. Briefly, W protein-Firefly luciferase (Luc, negative
226 control) dual expression plasmid EYFP constructs were transfected into HEK293T cells, and, 48 hrs
227 later, EYFP positive cells were sorted and incubated (48 hrs) prior to extracting and sequencing
228 mRNAs (Fig. 6A). This process was repeated in triplicate for each sample (GEO accession number:
229 SRP116105). The consistency of replicate data is highlighted by the Pearson correlation analysis in
230 which each set of three replicates can be seen clustered together (Fig. 6B). First, we assessed the
231 differentially expressed genes, identifying 216, 708, and 308 differentially expressed genes using the
232 Cuffdiff, EdgeR, and DESeq2 algorithms, respectively (53–55) (Fig. 6C). For subsequent analyses we
233 considered only the 114 genes identified by all three algorithms (Figs. 6C and D; Supplementary Table
234 1). The differential gene expression for W vs. Luc samples identified by RNA seq was then validated
235 by qRT-PCR (Fig. 6E). To accomplish this, we selected representative genes that were either down-
236 regulated (*INHBA* and *HSP6*) or upregulated (*WFIKKN2*, *MUC19*, and *OR2B67*). Interestingly, a GO
237 analysis of the 114 differentially expressed genes (W vs. Luc) revealed strong enrichment for terms

238 associated with DNA packing, stability, and innate immune defense (Table 3). These data suggest that
239 the W protein interferes with the PRP19 complex in terms of genomic maintenance, or disrupts the
240 innate antiviral response by altering gene regulation. Next, we sought to study the influence of nuclear
241 localization on gene expression. Briefly, 48 hrs after transfecting HEK293T cells with W, V, or
242 luciferase, mRNAs were extracted and the expression levels of *INHBA* and *MUC19* analyzed by qRT-
243 PCR. Despite an experimental design that excluded the selection of EYFP positive cells, and was
244 restricted to a 48 hr incubation post-transfection, the Nipah virus W protein induced a down-regulation
245 of *INHBA* and up regulation of *MUC19* (vs. the luciferase samples). In accordance with the p53 activity
246 assay results, the V protein was incapable of altering the expression of any of the selected genes (Fig.
247 6F), indicating that nuclear localization is essential if gene expression is to be altered. Analyses of the
248 differentially expressed transcripts (Supplementary Table 2), together with the variation in transcript
249 abundance (Fig. 6G) for W vs. Luc, did not suggest a modification of cellular splicing in the presence
250 of the Nipah virus W protein.
251
252 **DICER1-TARBP2 interactions with Nipah virus** matrix protein**.** We were also extremely interested
253 in the putative interactions identified in the TAP-MS experiments between the Nipah virus M protein
254 and the DICER1-TARBP2 complex (Fig. 2 and Fig. 7A). DICER1 participates primarily in the
255 biogenesis of (multiple classes of) small RNAs including miRNAs (56). However, other functions have
256 been attributed to this complex that include the processing of tRNAs and exogenous RNAs (57). To
257 corroborate our TAP-MS data we transfected HEK293T cells with the TAP-tagged versions of the M
258 (Nt and Ct tagged) and the V protein, After 24 hrs, endogenous DICER1 was immunoprecipitated and
259 probed with the Flag tag (inversely to the MS-TAP approach where the bait was the Nipah M protein)
260 (Fig. 7B left panel). Experiment that was repeated with HA-tagged M or V plasmids and including RFP
261 as an additional negative control (Fig. 7 middle and right panels). As in the TAP-MS experiments, N-

terminal tagged M was found to interact with DICER1 (Fig. 7B). At this point, we asked whether the Nipah virus M protein could influence DICER1 function. However, a luciferase-based DICER1 activity assay, with maturation analyses of exogenous miRNAs (Figs. 7C and D, respectively), showed that the M protein had no influence on the canonical functions of DICER1. Nonetheless, a role for M protein in other DICER1-TARBP2 activities cannot yet be ruled out.

Discussion

Currently, only a few sporadic cases of Nipah virus human infection are reported each year. However, the potential for human-to-human transmission, and an elevated pathogenicity, makes this virus a major potential global health threat. Accordingly, Nipah virus has been classified as a biosafetely level 4 (BSL4) pathogen. Surprisingly, few efforts have been made towards the development of a therapeutic or prophylactic treatment. In terms of antivirals, there are two main approaches. Historically, virologists have focused on the design of compounds that target viral proteins, and this approach has seen many successes. However, this strategy can present some disadvantages. For example, rapidly evolving viruses, such as RNA viruses, may develop drug resistance over a relatively short time period. In some cases (e.g. the neuraminidase inhibitors of the Influenza A virus) the antiviral compound interferes with a viral protein/process at a late stage of the viral life cycle. This type of late blockade can severely reduce drug efficacy and narrow the treatment window. These and other hurdles have prompted a strategic shift towards examining, and potentially targeting, host-proteins that are manipulated by the virus in order to fulfill a productive viral life cycle. By interfering with these interactions, either functionally (i.e. disrupting the host protein function) or upstream, by blocking the host-pathogen PPI, viral propagation might be reduced or even stopped. In the current work, we focused on identifying PPIs between human proteins and the Nipah virus. Our detailed TAP-MS

analyses revealed 101 PPIs, most of them previously unreported. These interactions represent a valuable set of potential drug targets for the treatment of Nipah virus infection. Further, by utilizing the DRUGBANK database we could explore the drug-ability of our interactor dataset, and provide a list of potential strategies to counter viral infection. It is important to mention that the experiments presented in this work were not conducted in a viral infection context. Transient expression from a plasmid-driven system yields large quantities of proteins which might alter the cellular interactome. Therefore, any result should be validated in a viral context before the functional relevance of the described PPIs is concluded.

The Nipah virus W protein participates in evading the innate immune response by binding STAT1 and preventing its phosphorylation in response to IFN. Additionally, protein W has been reported to block the TLR and RLR pathways. Here, we report a previously undetected interaction between the Nipah virus W protein and the PRP19 complex. Most likely, this interaction occurs through the N terminal region of the protein that is shared with the V and P proteins. All three proteins (W, V, and P) have the potential to interact with the PRP19 complex, as shown by our TAP-MS experiments. However, *in vivo*, only the W protein was able to co-localize with PLRG1 (a member of the PRP19 complex). Furthermore, only the Nipah virus W protein was capable of modulating cellular processes that are controlled (partially) by the PRP19 complex. These results indicate that the interactions between P, V, and the PRP19 complex that were captured in our MS-TAP and pull-down assays, may have occurred post cell lysis.

Our results showed a change in p53 activity and gene expression in the presence of the Nipah virus W protein. These changes correlate with the nuclear localization of the protein, as analyses of mutated V and W proteins revealed. The Nipah virus V protein, despite its capacity to interact with the PRP19

309 complex, could neither alter p53 activity nor gene expression when compared to controls. However,
310 when localized to the nucleus, we detected a restoration of the ability of the V protein to activate p53.
311
312 We should mention that our RNA sequencing data (differential expression of transcripts, and transcript
313 abundance for W vs. Luc samples) suggested no major modification of cellular splicing in the presence
314 of W. Nonetheless, collectively, our data indicates that the Nipah virus W protein is capable of altering
315 the function of the PRP19 complex, and that its nuclear localization is required for this activity.
316 Furthermore, the binding of STAT1 does not seem to be related to these effects, as indicated by our
317 analyses of the STAT1 binding deficient V and W proteins. These data suggest that further analyses of
318 the persistence of the protein W-PRP19 complex interaction, in the context of a viral infection, are now
319 warranted.
320
321 Due to the multi functionality of the PRP19 complex, it is currently impossible to pinpoint (with the
322 present data) which of its multiple functions the virus is manipulating. Many viruses modulate the
323 cellular apoptotic response (58) and it is possible that Nipah virus could, at some point during its life
324 cycle, induce apoptosis by interfering with a negative regulator of p53 such as the PRP19 complex.
325 There is also an extensive literature on the viral modulation of cellular gene expression. The Nipah
326 virus interaction with PRP19 might represent an additional level of control over the cellular antiviral
327 response. Whether this gene regulation is specific for a particular set of genes or is dependent on the
328 genes expressed in the infected cell cannot yet be deduced (with the current data). It would be useful to
329 investigate the influence of the W protein on gene expression in cells treated with IFN or stimulated
330 with viral RNA. GO enrichment analyses revealed that the differentially expressed genes are linked
331 with the innate immune response, which leads us to think that the Nipah virus is selectively hampering
332 the cellular response to viral infection. However, besides the defense response, the gene set analyzed

seems to participate in DNA packing, chromatin organization, and silencing, which could indicate an indirect mechanism of altering the cellular response to viral infection. Since the PRP19 complex is heavily involved in genome maintenance and DNA stability (47), an enrichment of GO terms related to those functions could reflect the cellular response to the Nipah virus protein W - PRP19 complex interaction.

Finally, we focused on the DICER1-Nipah M PPI. This interaction was confirmed by the pull-down (PD) of endogenous DICER1 in the presence of TAP-tagged Nipah virus M protein and V protein (as a negative control). As expected, only Nt tagged Nipah virus M protein could be seen interacting with DICER1. To corroborate this result the DICER1 PD was repeated in the presence of the HA-tagged versions of the Nipah virus M protein and using the RFP and Nipah virus V protein as a negative controls. Once again, only the Nt tagged forms of the Nipah virus M protein were PD together with DICER1. However, when DICER1 activity, in terms of miRNA production, was assessed in the presence of protein M we detected no noticeable effects. Nonetheless, DICER1 has been described to participate in other functions. In a Nipah virus infection, DICER1 could conceivably act as a pattern recognition receptor, as described in [59]. In that context, the interaction of Nipah virus M with DICER1 could prevent the cellular recognition of the virus without altering DICER1's canonical function.

Our work suggests multiple new strands of research. Not only do we describe new PPIs between the Nipah virus and host, but we also identify new functions for the viral W and M proteins. These data constitute a significant advance in our understanding of Nipah virus biology and we anticipate that these results will contribute to the development of a much-needed antiviral treatment.

Materials and methods

Protein expression and purification. For the identification of Nipah-human PPIs, DNAs encoding each viral protein fused to a TAP tag sequence at either the amino- or carboxy- terminus were transfected into HEK293T cells. Briefly, 30 µg of DNA were added to 1.5 mL of Opti-MEM medium (Gibco) (solution A). Separately, 1.5 mL Opti-MEM was supplemented with Lipofectamine 2000 (Life technologies; 2 µL/µg DNA, solution B). Solutions A and B were then mixed and incubated at room temperature for at least 10 minutes. The mixture was then overlaid onto a 15 cm tissue culture dish. Approximately 24 hours post transfection, cells were harvested and washed with PBS (x3). Cells were then lysed with 300 µL of Lysis Buffer (30 mM Tris-HCl, 150 mM NaCl, 0.5 % NP-40, Protease inhibitor (cOmplete Protease Inhibitor Cocktail, Roche) and phosphatase inhibitor (PhosSTOP, Roche)), and the lysate passed through a 30-gauge syringe (x3). The cell extract was clarified by centrifugation (10 minutes 10,000 g) and the supernatant transferred to a new tube. Tandem affinity purification (TAP) was as described in (28). Briefly, Nipah proteins were transiently expressed (24-30 hrs) in HEK293T cells. Next, cells were lysed and viral proteins purified usind the Strep and Flag tags in tamdem. Protein digestion and identification (LC MSMS using an LTQ Orbitrap) was completed by the W.M. Keck Biotechnology Resource Laboratory (http://medicine.yale.edu/keck/index.aspx). Constructs analyzed by MS (# replicates): Empty (2), Nt-EYFP (2), EYFP-Ct (2), Nt-RFP (1), RFP-Ct (1), Nt-N (3), N-Ct (3), Nt-P (2), P-Ct (2), Nt-V (2), V-Ct (2), Nt-W (2), W-Ct (2), Nt-EYFP-C (2), C-EYFP-Ct (2), Nt-M (2), M-Ct (2), Nt-F (2), F-Ct (2), Nt-F + F-Ct (1*), Nt-G (2), G-Nt (2), Nt-G + G-Ct (1*). * Nt and Ct plasmids were mix (1:1). This samples were not included in the analysis of the tag position**.**

Selection criteria and the abundance of interacting proteins.

379 The MS data were filtered according to the following selection criteria. All pseudo genes, predicted
380 proteins, and immunoglobulin fragments were discarded. Common contaminants in MS experiments
381 such as Keratins and Trypsins were also eliminated. Next, those proteins purified with any of the
382 negative controls (EYFP, RFP, or empty plasmid) were deleted. To further eliminate common artifacts
383 we utilized the CRAPome database (29) of common protein contaminants (i.e. identified from negative
384 control experiments) identified in affinity purification experiments followed by MS. Only those
385 proteins with an experimentally obtained found/total ratio >5x CRAPome (ratio) were selected. Finally,
386 proteins that interacted with 3 or more Nipah virus proteins were discarded as contaminants from the
387 experimental conditions used in the affinity purification (in this analysis, the sequence similarities for
388 the viral P, V, and W proteins, led these to be assessed collectively (i.e. as one)). The abundance of each
389 interaction was estimated using the exponentially modified Protein Abundance Index (emPAI). The
390 emPAI value offers an approximate, label-free, quantification of the proteins in a mixture based on
391 protein coverage obtained by peptide matches in a database search (60). To compare the intensities
392 across experiments the emPAIs for each protein were divided by the median emPAI value of the sample
393 (emPAI/med). As some hits were obtained 2, 3, 4, or up to 5 times, comparisons were made using the
394 average log (emPAI/med).
395
396 **Cell culture.** Colon epithelial carcinoma cells (HCT116), human alveolar epithelial cells (A549), and
397 human embryonic kidney 293T (HEK293T) cells were obtained from the American Type Culture
398 Collection and authenticated by Bioidentity (www.http://bioidentity.es). Cells were cultured in
399 Dulbecco's modified Eagle's medium (DMEM) (Gibco) supplemented with 10% fetal bovine serum
400 (FBS) (HyClone, Thermoscientific), and 1% penicillin-streptomycin (P/S) (Gibco). All cells were
401 grown at 37°C, 5% CO_2. Mycoplasma contamination analysis of the cells was performed by the Tissue
402 culture core facility at the Universitat de València.

403

404 **p53 reporter assay.** HCT116 and A549 cells were transfected (Lipofectamine 2000) with a p53
405 reporter plasmid (50) (Addgene plasmid 16442, http://www.addgene.org), a pRL-SV40 vector
406 (Promega, http://www.promega.com; included to normalize the measurements), and a plasmid carrying
407 the protein of interest. To induce p53 activation, 24 hrs after transfection, cells were either infected with
408 Newcastle Disease virus (NDV) or were exposed to Doxorubicin (0.2 - 0.4 μM, Calbiochem,
409 http://www.emdmillipore.com). Twenty-four hours later, cells were lysed and the luciferase signal from
410 Firefly Renilla luciferase measured using a Dual-Luciferase Reporter Assay System (Promega,
411 http://www.promega.com). NDV infections were as follows: twenty-four hours after transfection media
412 was removed and the cells washed with PBS. Infection was with 200 μL of PBS/0.5% BSA with NDV
413 at a MOI = 10. After a 1 hour incubation at room temperature, the virus was aspirated, and the cells
414 washed with PBS. Fresh media was then added to the cells.

415

416 **Sub-cellular protein localization**. For the co-localization study of PLRG1 and the Nipah virus W, V,
417 and P proteins, HEK293T cells were seeded onto poly-Lys treated cover slips and, approximately 20-24
418 hrs later, transfected with YFP-PLRG1 and either the P, V, or W (flag-tagged) constructs. After 24 hrs,
419 cells were fixed (paraformaldehyde 4%, 20 min), permeabilized (0.1% Triton X-100) and washed (3x,
420 PBS). Immunofluorescence was with a mouse anti-flag antibody (Sigma-Aldrich,
421 www.sigmaaldrich.com); the secondary antibody was an anti-mouse Alexa 647 conjugate (Sigma-
422 Aldrich), with DAPI used to stain nuclei (Fluoroshield, Sigma-Aldrich). Images were captured using a
423 FV1000 confocal microscope (Olympus, http://www.olympus-lifescience.com) at the microscopy core
424 facility of the University of Valencia.

425

426 **Immunoprecipitation and immunodetection.** Cells were transfected with the appropriated protein

(M, V or RFP) bearing the indicated antibody tag (HA or Flag). Approximately 48 hrs later, cells were lysed (20 mM Tris (pH 7.5), 150 mM NaCl, 1 mM EDTA, 1 mM EGTA, 1% Triton X-100, 2.5 mM Sodium pyrophosphate, 1 mM Na_3VO_4, 1x Cocktail protease (Pierce)) on ice (5 min). Samples were centrifuged (10 min at 14,000 g) and the supernatant pre-cleared by a 30 - 60 min incubation (at 4 ºC) with protein A. Protein A was then pelleted by centrifugation (2,500 g 2-3min) and 1-10 µg of anti-DICER1 antibody added to the clarified supernatant (Abcam Ab14601; incubated at 4 ºC overnight). Next, 20 µL of Protein A was added, and the samples incubated for 1 hr at 4ºC, then passed through a micro-spin column. Columns were washed (x3) with lysis buffer. Finally, samples were incubated with elution buffer (0.2 M glycine-HCl at pH 2.5) for 10 min at room temperature and then centrifuged (2 min at 2,500 g). Flow-throughs were subject to western blot using either an anti-HA or an anti-Flag antibody (Sigma-Aldrich). For the identification of BCAS2, PRP19, and CDC5L, we used the WH0010286M1, SAB4501215, and HPA011361 antibodies, respectively (Sigma-Aldrich).

DICER1 luciferase activity assay. To explore the activity of DICER1 in the presence of the Nipah virus W protein we used a luciferase assay based on miR124 processing. Briefly, a pBT plasmid expressing Gaussia luciferase containing four miR124 target sites was transfected into HEK293T cells together with a pEM plasmid containing miR124. An empty pEM plasmid was used as a negative control. Successful production of mature miR124 via DICER1 should block luciferase expression. Conversely, if DICER1 activity is diminished, the level of the luciferase signal should increase.

RNAseq and analyses. Sequencing and sample preparation were completed at the Genomics Core facility at the University of Valencia. Prior to sequencing, the appropriate RNA quality was verified using a Bioanalyzer (Agilent, http://www.agilent.com) with the Agilent RNA 6000 Nano kit (used according to the manufacturer's instructions). RNA libraries were prepared using the TruSeq Stranded

mRNA sample preparation kit (Illumina, www.illumina.com) following the manufacturer's specifications. Sequencing was with an Illumina NextSeq5000 sequencer using the High Output kit (Illumina) (GEO accession number: SRP116105). Data analyses were with CuffDiff (53), EdgeR (54), and the DESeq2 (55) software.

Acknowledgements

We would like to thank to Drs. M. Shaw, CF Basler, BR tenOever, and BH Lee for plasmids and reagents. We thank Dr. A. Lamond for the YFP-PLRG1 construct. We also thank Dr. M Sanchez del Pino for his advice on the analysis of the proteomic data. The RNA sequencing was performed by the Genomics Core facility at the Universitat de València. This work was supported by grants from the Spanish Ministry of Economy and Competitiveness (MINECO) (grant no. BFU2016-79487), and from the Generalitat Valenciana (GV/2016/139, Program *Grupos Emergentes*; and PROMETEOII/2014/061, Program *Grupos de Excelencia*). LMG is funded by the Spanish MiNECO (Program *Juan de la Cierva*).

LMG designed research; LMG and NMVV performed research; LMG and IM analyzed data and wrote the paper.

The authors declare no competing financial interests.

Bibliography

1. Aguilar HC, Lee B. 2011. Emerging paramyxoviruses: molecular mechanisms and antiviral

strategies. Expert Rev Mol Med 13:e6.

2. Wong KT, Shieh WJ, Zaki SR, Tan CT. 2002. Nipah virus infection, an emerging paramyxoviral zoonosis. Springer Semin Immunopathol 24:215–228.

3. Lee KE, Umapathi T, Tan CB, Tjia HT, Chua TS, Oh HM, Fock KM, Kurup A, Das A, Tan AK, Lee WL. 1999. The neurological manifestations of Nipah virus encephalitis, a novel paramyxovirus. Ann Neurol 46:428–432.

4. Rockx B, Winegar R, Freiberg AN. 2012. Recent progress in henipavirus research: molecular biology, genetic diversity, animal models. Antiviral Res 95:135–149.

5. Escaffre O, Borisevich V, Rockx B. 2013. Pathogenesis of Hendra and Nipah virus infection in humans. J Infect Dev Ctries 7:308–311.

6. Clayton BA. 2017. Nipah virus: transmission of a zoonotic paramyxovirus. Curr Opin Virol 22:97–104.

7. Luby SP, Hossain MJ, Gurley ES, Ahmed BN, Banu S, Khan SU, Homaira N, Rota PA, Rollin PE, Comer JA, Kenah E, Ksiazek TG, Rahman M. 2009. Recurrent zoonotic transmission of Nipah virus into humans, Bangladesh, 2001-2007. Emerg Infect Dis 15:1229–1235.

8. Negrete OA, Levroney EL, Aguilar HC, Bertolotti-Ciarlet A, Nazarian R, Tajyar S, Lee B. 2005. EphrinB2 is the entry receptor for Nipah virus, an emergent deadly paramyxovirus. Nature 436:401–405.

9. Negrete OA, Wolf MC, Aguilar HC, Enterlein S, Wang W, Mühlberger E, Su SV, Bertolotti-Ciarlet A, Flick R, Lee B. 2006. Two key residues in ephrinB3 are critical for its use as an alternative receptor for Nipah virus. PLoS Pathog 2:e7.

10. Dhondt KP, Mathieu C, Chalons M, Reynaud JM, Vallve A, Raoul H, Horvat B. 2013. Type I

interferon signaling protects mice from lethal henipavirus infection. J Infect Dis 207:142–151.

11. Satterfield BA, Cross RW, Fenton KA, Borisevich V, Agans KN, Deer DJ, Graber J, Basler CF, Geisbert TW, Mire CE. 2016. Nipah Virus C and W Proteins Contribute to Respiratory Disease in Ferrets. J Virol 90:6326–6343.

12. Basler CF. 2012. Nipah and hendra virus interactions with the innate immune system. Curr Top Microbiol Immunol 359:123–152.

13. Park M-S, Shaw ML, Muñoz-Jordan J, Cros JF, Nakaya T, Bouvier N, Palese P, García-Sastre A, Basler CF. 2003. Newcastle disease virus (NDV)-based assay demonstrates interferon-antagonist activity for the NDV V protein and the Nipah virus V, W, and C proteins. J Virol 77:1501–1511.

14. Shaw ML. 2009. Henipaviruses employ a multifaceted approach to evade the antiviral interferon response. Viruses 1:1190–1203.

15. Ludlow LE, Lo MK, Rodriguez JJ, Rota PA, Horvath CM. 2008. Henipavirus V protein association with Polo-like kinase reveals functional overlap with STAT1 binding and interferon evasion. J Virol 82:6259–6271.

16. Rodriguez JJ, Parisien J-P, Horvath CM. 2002. Nipah virus V protein evades alpha and gamma interferons by preventing STAT1 and STAT2 activation and nuclear accumulation. J Virol 76:11476–11483.

17. Rodriguez JJ, Cruz CD, Horvath CM. 2004. Identification of the nuclear export signal and STAT-binding domains of the Nipah virus V protein reveals mechanisms underlying interferon evasion. J Virol 78:5358–5367.

18. Shaw ML, García-Sastre A, Palese P, Basler CF. 2004. Nipah virus V and W proteins have a common STAT1-binding domain yet inhibit STAT1 activation from the cytoplasmic and nuclear compartments, respectively. J Virol 78:5633–5641.

19. Andrejeva J, Childs KS, Young DF, Carlos TS, Stock N, Goodbourn S, Randall RE. 2004. The V proteins of paramyxoviruses bind the IFN-inducible RNA helicase, mda-5, and inhibit its activation of the IFN-beta promoter. Proc Natl Acad Sci U S A 101:17264–17269.

20. Childs K, Stock N, Ross C, Andrejeva J, Hilton L, Skinner M, Randall R, Goodbourn S. 2007. mda-5, but not RIG-I, is a common target for paramyxovirus V proteins. Virology 359:190–200.

21. Parisien J-P, Bamming D, Komuro A, Ramachandran A, Rodriguez JJ, Barber G, Wojahn RD, Horvath CM. 2009. A shared interface mediates paramyxovirus interference with antiviral RNA helicases MDA5 and LGP2. J Virol 83:7252–7260.

22. Shaw ML, Cardenas WB, Zamarin D, Palese P, Basler CF. 2005. Nuclear localization of the Nipah virus W protein allows for inhibition of both virus- and toll-like receptor 3-triggered signaling pathways. J Virol 79:6078–6088.

23. Bharaj P, Wang YE, Dawes BE, Yun TE, Park A, Yen B, Basler CF, Freiberg AN, Lee B, Rajsbaum R. 2016. The Matrix Protein of Nipah Virus Targets the E3-Ubiquitin Ligase TRIM6 to Inhibit the IKKε Kinase-Mediated Type-I IFN Antiviral Response. PLoS Pathog 12:e1005880.

24. Ding S, Mooney N, Li B, Kelly MR, Feng N, Loktev AV, Sen A, Patton JT, Jackson PK, Greenberg HB. 2016. Comparative Proteomics Reveals Strain-Specific β-TrCP Degradation via Rotavirus NSP1 Hijacking a Host Cullin-3-Rbx1 Complex. PLoS Pathog 12:e1005929.

25. Hirohata Y, Kato A, Oyama M, Kozuka-Hata H, Koyanagi N, Arii J, Kawaguchi Y. 2015. Interactome analysis of herpes simplex virus 1 envelope glycoprotein H. Microbiol Immunol 59:331–337.

26. Sangsuriya P, Huang J-Y, Chu Y-F, Phiwsaiya K, Leekitcharoenphon P, Meemetta W, Senapin S, Huang W-P, Withyachumnarnkul B, Flegel TW, Lo C-F. 2014. Construction and application of a protein interaction map for white spot syndrome virus (WSSV). Mol Cell Proteomics MCP

13:269–282.

27. Tarassov K, Messier V, Landry CR, Radinovic S, Serna Molina MM, Shames I, Malitskaya Y, Vogel J, Bussey H, Michnick SW. 2008. An in vivo map of the yeast protein interactome. Science 320:1465–1470.

28. Gloeckner CJ, Boldt K, Schumacher A, Roepman R, Ueffing M. 2007. A novel tandem affinity purification strategy for the efficient isolation and characterisation of native protein complexes. Proteomics 7:4228–4234.

29. Mellacheruvu D, Wright Z, Couzens AL, Lambert J-P, St-Denis NA, Li T, Miteva YV, Hauri S, Sardiu ME, Low TY, Halim VA, Bagshaw RD, Hubner NC, Al-Hakim A, Bouchard A, Faubert D, Fermin D, Dunham WH, Goudreault M, Lin Z-Y, Badillo BG, Pawson T, Durocher D, Coulombe B, Aebersold R, Superti-Furga G, Colinge J, Heck AJR, Choi H, Gstaiger M, Mohammed S, Cristea IM, Bennett KL, Washburn MP, Raught B, Ewing RM, Gingras A-C, Nesvizhskii AI. 2013. The CRAPome: a contaminant repository for affinity purification-mass spectrometry data. Nat Methods 10:730–736.

30. Harcourt BH, Tamin A, Ksiazek TG, Rollin PE, Anderson LJ, Bellini WJ, Rota PA. 2000. Molecular characterization of Nipah virus, a newly emergent paramyxovirus. Virology 271:334–349.

31. Horie R, Yoneda M, Uchida S, Sato H, Kai C. 2016. Region of Nipah virus C protein responsible for shuttling between the cytoplasm and nucleus. Virology 497:294–304.

32. Pentecost M, Vashisht AA, Lester T, Voros T, Beaty SM, Park A, Wang YE, Yun TE, Freiberg AN, Wohlschlegel JA, Lee B. 2015. Evidence for ubiquitin-regulated nuclear and subnuclear trafficking among Paramyxovirinae matrix proteins. PLoS Pathog 11:e1004739.

33. Law V, Knox C, Djoumbou Y, Jewison T, Guo AC, Liu Y, Maciejewski A, Arndt D, Wilson M,

Neveu V, Tang A, Gabriel G, Ly C, Adamjee S, Dame ZT, Han B, Zhou Y, Wishart DS. 2014. DrugBank 4.0: shedding new light on drug metabolism. Nucleic Acids Res 42:D1091-1097.

34. Wishart DS, Knox C, Guo AC, Shrivastava S, Hassanali M, Stothard P, Chang Z, Woolsey J. 2006. DrugBank: a comprehensive resource for in silico drug discovery and exploration. Nucleic Acids Res 34:D668-672.

35. Orchard S, Ammari M, Aranda B, Breuza L, Briganti L, Broackes-Carter F, Campbell NH, Chavali G, Chen C, del-Toro N, Duesbury M, Dumousseau M, Galeota E, Hinz U, Iannuccelli M, Jagannathan S, Jimenez R, Khadake J, Lagreid A, Licata L, Lovering RC, Meldal B, Melidoni AN, Milagros M, Peluso D, Perfetto L, Porras P, Raghunath A, Ricard-Blum S, Roechert B, Stutz A, Tognolli M, van Roey K, Cesareni G, Hermjakob H. 2014. The MIntAct project—IntAct as a common curation platform for 11 molecular interaction databases. Nucleic Acids Res 42:D358–D363.

36. Szklarczyk D, Franceschini A, Wyder S, Forslund K, Heller D, Huerta-Cepas J, Simonovic M, Roth A, Santos A, Tsafou KP, Kuhn M, Bork P, Jensen LJ, von Mering C. 2015. STRING v10: protein-protein interaction networks, integrated over the tree of life. Nucleic Acids Res 43:D447-452.

37. Pichlmair A, Kandasamy K, Alvisi G, Mulhern O, Sacco R, Habjan M, Binder M, Stefanovic A, Eberle C-A, Goncalves A, Bürckstümmer T, Müller AC, Fauster A, Holze C, Lindsten K, Goodbourn S, Kochs G, Weber F, Bartenschlager R, Bowie AG, Bennett KL, Colinge J, Superti-Furga G. 2012. Viral immune modulators perturb the human molecular network by common and unique strategies. Nature 487:486–490.

38. Bauer A, Neumann S, Karger A, Henning A-K, Maisner A, Lamp B, Dietzel E, Kwasnitschka L, Balkema-Buschmann A, Keil GM, Finke S. 2014. ANP32B is a nuclear target of henipavirus M proteins. PloS One 9:e97233.

39. Parvege MM, Rahman M, Nibir YM, Hossain MS. 2016. Two highly similar LAEDDTNAQKT and LTDKIGTEI epitopes in G glycoprotein may be useful for effective epitope based vaccine design against pathogenic Henipavirus. Comput Biol Chem 61:270–280.

40. Popa A, Carter JR, Smith SE, Hellman L, Fried MG, Dutch RE. 2012. Residues in the hendra virus fusion protein transmembrane domain are critical for endocytic recycling. J Virol 86:3014–3026.

41. Bonaparte MI, Dimitrov AS, Bossart KN, Crameri G, Mungall BA, Bishop KA, Choudhry V, Dimitrov DS, Wang L-F, Eaton BT, Broder CC. 2005. Ephrin-B2 ligand is a functional receptor for Hendra virus and Nipah virus. Proc Natl Acad Sci U S A 102:10652–10657.

42. Sun W, McCrory TS, Khaw WY, Petzing S, Myers T, Schmitt AP. 2014. Matrix proteins of Nipah and Hendra viruses interact with beta subunits of AP-3 complexes. J Virol 88:13099–13110.

43. Ciancanelli MJ, Volchkova VA, Shaw ML, Volchkov VE, Basler CF. 2009. Nipah virus sequesters inactive STAT1 in the nucleus via a P gene-encoded mechanism. J Virol 83:7828–7841.

44. Mahajan K. 2016. hPso4/hPrp19: a critical component of DNA repair and DNA damage checkpoint complexes. Oncogene 35:2279–2286.

45. Cheng SC, Tarn WY, Tsao TY, Abelson J. 1993. PRP19: a novel spliceosomal component. Mol Cell Biol 13:1876–1882.

46. Chanarat S, Seizl M, Sträßer K. 2011. The Prp19 complex is a novel transcription elongation factor required for TREX occupancy at transcribed genes. Genes Dev 25:1147–1158.

47. Xu Q, Wang F, Xiang Y, Zhang X, Zhao Z-A, Gao Z, Liu W, Lu X, Liu Y, Yu X-J, Wang H, Huang J, Yi Z, Gao S, Li L. 2015. Maternal BCAS2 protects genomic integrity in mouse early embryonic development. Dev Camb Engl 142:3943–3953.

48. Chen P-H, Lee C-I, Weng Y-T, Tarn W-Y, Tsao Y-P, Kuo P-C, Hsu P-H, Huang C-W, Huang C-S, Lee H-H, Wu J-T, Chen S-L. 2013. BCAS2 is essential for Drosophila viability and functions in pre-mRNA splicing. RNA N Y N 19:208–218.

49. Kleinridders A, Pogoda H-M, Irlenbusch S, Smyth N, Koncz C, Hammerschmidt M, Brüning JC. 2009. PLRG1 is an essential regulator of cell proliferation and apoptosis during vertebrate development and tissue homeostasis. Mol Cell Biol 29:3173–3185.

50. el-Deiry WS, Tokino T, Velculescu VE, Levy DB, Parsons R, Trent JM, Lin D, Mercer WE, Kinzler KW, Vogelstein B. 1993. WAF1, a potential mediator of p53 tumor suppression. Cell 75:817–825.

51. Hientz K, Mohr A, Bhakta-Guha D, Efferth T. 2017. The role of p53 in cancer drug resistance and targeted chemotherapy. Oncotarget 8:8921–8946.

52. Palese P, Shaw ML. 2007. Fields Virology. Orthomyxoviridae Viruses Their Replication 5th Edn Phila PA Lippincott Williams Wilkins Wolters Kluwer Bus 1647–1689.

53. Love MI, Huber W, Anders S. 2014. Moderated estimation of fold change and dispersion for RNA-seq data with DESeq2. Genome Biol 15.

54. Robinson MD, McCarthy DJ, Smyth GK. 2010. edgeR: a Bioconductor package for differential expression analysis of digital gene expression data. Bioinformatics 26:139–140.

55. Trapnell C, Williams BA, Pertea G, Mortazavi A, Kwan G, van Baren MJ, Salzberg SL, Wold BJ, Pachter L. 2010. Transcript assembly and quantification by RNA-Seq reveals unannotated transcripts and isoform switching during cell differentiation. Nat Biotechnol 28:511–515.

56. Svobodova E, Kubikova J, Svoboda P. 2016. Production of small RNAs by mammalian Dicer. Pflugers Arch 468:1089–1102.

57. Song M-S, Rossi JJ. 2017. Molecular mechanisms of Dicer: endonuclease and enzymatic activity. Biochem J 474:1603–1618.

58. Galluzzi L, Brenner C, Morselli E, Touat Z, Kroemer G. 2008. Viral control of mitochondrial apoptosis. PLoS Pathog 4:e1000018.

59. Rawling DC, Pyle AM. 2014. Parts, assembly and operation of the RIG-I family of motors. Curr Opin Struct Biol 25:25–33.

60. Ishihama Y, Oda Y, Tabata T, Sato T, Nagasu T, Rappsilber J, Mann M. 2005. Exponentially Modified Protein Abundance Index (emPAI) for Estimation of Absolute Protein Amount in Proteomics by the Number of Sequenced Peptides per Protein. Mol Cell Proteomics 4:1265–1272.

Figure legends

Figure 1. Affinity purification of Nipah virus proteins and analyses of MS data. (**A**) Flowchart of the TAP-MS approach used to identify Nipah virus-human interactions. hpt denotes hours post transfection. (**B**) The ave log (emPAI/med) of the 101 PPIs were grouped according to the number of times (replicates) they were found (2, 3, or 4). The single PPI found in 5 replicates was excluded from the representation. For each group, values for the number of interactors (top) and the averaged value of the ave log (emPAI/med) are shown. Those proteins found in 2 replicates were color-coded based on the TAP-tag position in the bait: blue, Nt; green, Ct; black (either Nt or Ct). The averaged values of the ave log (emPAI/med) of tag-position dependent (tpd) and independent (tpi) interactions are also indicated. (**C**) Influence of tag position on identification of the PPI. The number of interactors for each bait (Nipah virus proteins N, P, V, W, C, M, F, and G) are shown. Bars are color-coded according to the location of the tag. Gray indicates a host protein identified using a bait tagged at either terminus; blue indicates a protein that bound bait tagged at its N terminus (Nt) exclusively; green indicates the

opposite, an interaction between host protein and bait tagged exclusively at the C terminus (Ct). The pie chart above the bar graph indicates the percentage of interactors identified with Nt (blue), Ct (green), or Nt and Ct (gray) tagged baits. (**D** and **E**) Heat maps representing enriched cellular components (**D**) and biological processes (**E**) deduced from the human proteins captured with the Nipah virus baits. ER denotes Endoplasmic Reticulum. (**F**) The percentage of PPIs identified in the TAP-MS experiment that have been shown to be related (in the literature) to viral infection. Significance (Fisher test) was calculated using a random list of 101 proteins as a reference set.

Figure 2. Network representation of TAP-MS-identified Nipah virus-human PPIs. A total of 126 interactions (edges) and 93 proteins (nodes) are represented. Newly identified PPIs are indicated by solid black lines; previously described PPIs are those highlighted with a double solid line. Gray dotted lines indicate human-human PPIs obtained from the String and intACT databases. Nipah virus proteins are shown light red. Cellular proteins are shown either blue (Nt) or green (Ct) depending on the tag position (as described previously). Protein names (obtained from Uniprot) are provided within each node.

Figure 3. Nipah virus proteins W and V interact with STAT4. (**A**) TAP of tagged V, W, V_{G121E}, W_{G121E}, and EYFP. Post purification, samples were immuno-blotted for STAT1, STAT4, and the FLAG tag. (**B**) Network representation of the Nipah virus V and W interactions with STAT family members, as obtained in the TAP-MS experiments. TAP of tagged V, W, V_{G121E}, W_{G121E} and EYFP. After purification samples were probed against STAT1, STAT4 and FLAG.

Figure 4. Interactions between the Nipah virus and the PRP19 complex. (**A**) Network representation of TAP-MS identified interactions between PRP19 complex members (gray nodes) and

Nipah virus proteins (red nodes). Solid black lines indicate interactions found in the TAP-MS experiments. Gray dotted lines represent PPIs identified in the String and intACT databases. (**B**). Average log(emPAI/median) value of the experimentally found interactions. Red dots highlight the PRP19 complex associated proteins. The dotted line indicates the average value for all samples. (**C**) Western blot identification of PRP19 complex members. Wildtype and mutant (G121E) V and W lysates, together with EYFP, were TAP purified and the final eluates immuno-blotted for CDC5L, PRP19, PLRG1, BCAS2, and the Flag tag. (**D**) Cellular localization of the V, W, and P proteins (red, immune-labeled) with YFP-PLRG1 (green). DAPI staining is shown as light gray. Co-localization of red and green channels is highlighted in yellow. Arrowheads indicate peri-nuclear regions where green and red co-localization was found.

Figure 5. Nipah virus modulation of p53 activity. To investigate p53 activity in the presence of Nipah virus protein, a luciferase reporter plasmid was transfected into HCT116 cells **(A-C)** and A549 **(D-F)**. Post transfection cells were left untreated (Untreated) (**A** and **D**), were infected with Newcastle disease virus (NDV) (**B** and **E**) or were exposed to doxorubicin (Doxorubicin) (**C** and **F**). Luciferase values for control (untreated) cells transfected with the p53 reporter and EYFP were used to normalize the data (100%, dotted line, white bar panel **A**). Error bars indicate the standard deviation of at least three replicates. Significance (t-test) in each panel was calculated by comparison with values obtained with the Nipah virus W samples (black bar). *: p value<0.05, **: p value<0.01, ***: p value<0.001, ns: not significant.

Figure 6. Nipah virus modulation of gene expression. (**A**) Flowchart representation of the mRNA extraction and purification protocol. (**B**) Pearson correlation analyses of the sequenced samples. This analysis included the expression profiles of all of the genes. (**C**) Venn diagram indicating the number of

differentially expressed genes when comparing Nipah virus W and luciferase samples, identified by CuffDiff (pink), DESeq2 (light blue), and EdgeR (yellow). (**D**) Heat map of the Log_2RPM values for the 114 differentially expressed genes detected by all three algorithms. (**E**) qRT-PCR validation of RNA seq data. The bar graph shows the fold induction provoked by the expression of W protein over the luciferase values. Error bars represent the standard deviation of the three replicates. (**F**) qRT-PCR measurements of *INHBA* (red) and *MUC19* (green) mRNAs, selected as example of genes down and up regulated, respectively, by the Nipah virus W protein. In these experiments cells were transfected with luciferase (reference sample) and expression plasmids for either the W or V proteins. After 48 hrs, mRNAs were extracted and measured by qRT-PCR. The bar graph shows the fold induction of mRNA achieved in the presence of either the W or V protein, over values recorded for luciferase. Error bars indicate the standard deviation of three replicates. Significance (t-test) was calculated by comparing the V and W samples. * denotes a p value <0.05 . (**G**) Average Log2 RPM for the Luc and W sample.

Figure 7. Interaction of Nipah virus M with the DICER1-TARBP2 complex. (**A**) Network representation of the Nipah virus M protein interaction with cellular proteins. (**B**) Left panel, immunoprecipitation of endogenous DICER1 in HEK293T cells transfected with Nipah virus M and V protein (M-TAP and TAP-M and V-TAP) (TAP tagged either at the amino terminus, TAP-M or the carboxilo end M-TAP and V-TAP). Middle and left panel show immunoprecipitation of endogenous DICER1 in HEK293T cells transfected with Nipah virus M and V protein and the RFP tagged with and HA flag in the indicated terminus. (**C**) DICER1 activity assay. HEK293T cells were transfected with luciferase (luc) plasmids containing mir124 target sites plus a plasmid expressing mir124. In the absence of mature miR124, expression of Luc is unhampered. Conversely, DICER1 dependent production of mature miR124 blocks Luc expression. The black bar indicates a negative control, comprising cells expressing Luc but no miR124 plasmid. White bars include EYFP (positive) and W

samples. A western blot was included to confirm the expression of EYFp and the Nipah virus M protein. (**D**) Northern blot of pre- and mature miR124 in cells expressing EYFP or the Nipah virus M protein.

Table 1. Proteins identified by the TAP-MS

Bait	Uniprot	Gene Name	Protein name	Replicates[a]	Found Ratio[b]	Nt[c]	Ct[c]	Ave log(empai/med)[d]	Reported in
W	O00505	KPNA3	Importin-alpha 3	3	0.75	1	2	1.59	22, 37
P	O75934	SPF27	Pre-mrna-splicing factor spf27	4	1.00	2	2	1.43	
P	Q9UMS4	PRP19	Pre-mrna-processing factor 19	4	1.00	2	2	1.37	
M	Q92688	ANP32B	Acidic leucine-rich nuclear phosphoprotein 32	2	0.50	1	1	1.28	38
W	O00629	KPNA4	Importin subunit alpha-4	4	1.00	2	2	1.26	22, 37
W	B2R7W3	BCAS2	Pre-mrna-splicing factor spf27	4	1.00	2	2	1.23	
W	Q9UMS4	PRP19	Pre-mrna-processing factor 19	4	1.00	2	2	1.19	
P	Q99459	CDC5L	Cell division cycle 5-like protein	4	1.00	2	2	1.18	
V	B2R7W3	BCAS2	Pre-mrna-splicing factor spf27	3	0.75	1	2	1.08	
V	P52630	STAT2	Signal transducer and activator of transcription 2	2	0.50	1	1	0.98	16, 37
V	Q9UMS4	PRP19	Pre-mrna-processing factor 19	4	1.00	2	2	0.94	
P	O43660	PLRG1	Pleiotropic regulator 1	4	1.00	2	2	0.89	
C	P40855	PEX19	Peroxisomal biogenesis factor 19 a	2	0.50	2	0	0.83	
F	Q53H37	CALM5	Calmodulin-like protein 5	2	0.40	0	2	0.80	
C	P35613	BSG	Basigin/cd147emmpirin	3	0.75	2	1	0.80	
V	O43660	PLRG1	Pleiotropic regulator 1	2	0.50	0	2	0.79	
F	Q9Y5M8	SRPRB	Signal recognition particle receptor subunit beta	3	0.60	1	1	0.78	
N	O75190	DNAJB6	Dnaj subfamily b member 6	2	0.33	1	1	0.76	
C	Q9UHG3	PCYOX1	Prenylcysteine lyase	2	0.50	2	0	0.73	
M	P49458	SRP9	Signal recognition particle 9 kda protein	2	0.50	1	1	0.67	
M	A0A024R2I7	RAD18	Postreplication repair protein hrad18p	4	1.00	2	2	0.67	32
W	O43660	PLRG1	Pleiotropic regulator 1	3	0.75	1	2	0.66	
F	I2G9F8	HLA-C	Major histocompatibility complex, class I-c	3	0.60	2	1	0.62	39*
F	P11441	UBL4A	Ubiquitin-like protein 4a	4	0.80	2	1	0.59	
P	P51116	FXR2	Fragile x mental retardation syndrome related protein	4	1.00	2	2	0.55	
V	P42771	CDKN2A	P16-ink4	2	0.50	1	1	0.48	
N	D3DR22	HSD17B12	Hydroxysteroid (17-beta) dehydrogenase 12	2	0.33	2	0	0.48	
C	O00161	SNAP23	Snap-23	2	0.50	2	0	0.47	
M	O15355	PPM1G	Protein phosphatase 1g	4	1.00	2	2	0.47	
V	Q99459	CDC5L	Cell division cycle 5-like protein	3	0.75	1	2	0.36	
G	P07203	GPX1	Glutathione peroxidase	2	0.40	1	1	0.33	
N	M4QFU4	HLA-B	Mhc class i antigen	2	0.33	0	2	0.33	39*
M	Q9UPY3	DICER1	Hypothetical helicase k12h4.8-like protein	2	0.50	0	2	0.30	
M	Q7Z6Z7	HUWE1	E3 ubiquitin-protein ligase huwe1	2	0.50	0	2	0.28	
M	Q8WVZ9	KBTBD7	Kelch repeat and btb domain-containing protein 7	2	0.50	1	1	0.27	
W	Q99459	CDC5L	Cell division cycle 5-like protein	3	0.75	1	2	0.26	
F	A0A024RBE6	NAP1L1	Nucleosome assembly protein 1-like 1, cra_b	2	0.40	0	2	0.25	
M	Q15633	TARBP2	Risc-loading complex subunit tarbp2 b	3	0.75	1	2	0.23	
C	Q9P0T7	TMEM9	Transmembrane protein 9	2	0.50	0	2	0.23	

N	O00217	NDUFS8	Nadh dehydrogenase iron-sulfur protein 8	2	0.33	2	0	0.22	
G	Q15768	EFNB3	Ephrin-b3	2	0.40	2	0	0.19	32
C	Q9H9H4	VPS37B	Vacuolar protein sorting-associated protein 37b	4	1.00	2	2	0.19	
V	Q13126	MTAP	Methylthioadenosine phosphorylase	3	0.75	1	2	0.18	
F	Q7L5D6	GET4	Cgi-20 protein	2	0.40	2	0	0.14	
F	A4D0U5	TES	Testin 1	4	0.80	2	2	0.14	
G	Q9UK22	FBX2	F-box protein fbx2	5	1.00	2	2	0.13	
N	Q9Y4R8	TELO2	Kiaa0683 protein	2	0.33	1	1	0.12	
F	Q3SY69	ALDH1L2	Aldehyde dehydrogenase 1 family, member l2	2	0.40	1	1	0.09	
M	Q9UL15	BAG5	Bag family molecular chaperone regulator 5	2	0.50	1	1	0.06	
P	O43709	WBSCR22	Uncharacterized methyltransferase wbscr22	2	0.50	1	1	0.05	
G	P27544	CERS1	Ceramide synthase 1	2	0.40	2	0	0.05	
G	O60613	SEP15	Selenoprotein 1 precursor	2	0.40	2	0	0.05	
C	Q9BRK5	SDF4	Calcium-binding protein 1 precursor	2	0.50	0	2	0.03	
F	P51648	ALDH3A2	Fatty aldehyde dehydrogenase 2	3	0.60	1	1	0.03	
F	Q96AY3	FKBP10	Fk506-binding protein	2	0.40	2	0	0.01	
N	Q8NBQ5	HSD17B11	Unnamed protein product	3	0.50	1	2	0.01	
P	P52630	STAT2	Signal transducer and activator of transcription 2	2	0.50	1	1	0.01	16, 37
F	P02786	TFRC	Transferrin receptor protein 1	3	0.60	2	1	0.00	40**
G	P52799	EFNB2	Ephrin-b2	2	0.40	2	0	-0.01	8, 41
M	Q6PEV8	FAM199X	Fam199x	2	0.50	0	2	-0.02	
M	Q9Y4B6	VPRBP	Vprbp 1	3	0.75	1	2	-0.04	42
G	Q9Y3A6	TMED5	Transmembrane emp24 protein transport	3	0.60	0	2	-0.06	
F	P46459	NSF	Vesicle-fusing atpase	2	0.40	2	0	-0.09	
C	P51648	ALDH3A2	Fatty aldehyde dehydrogenase 2	2	0.50	1	1	-0.09	
C	Q9NV96	TMEM30A	Cell cycle control protein 50a	2	0.50	0	2	-0.10	
F	Q9UNL2	SSR3	Translocon-associated protein subunit gamma	3	0.60	1	1	-0.10	
W	Q14765	STAT4	Signal transducer and activator of transcription 4	3	0.75	2	2	-0.10	
P	P56182	RRP1	Ribosomal Rna processing protein 1	2	0.50	1	1	-0.11	
M	Q9BTT0	ANP32E	Acidic leucine-rich nuclear phosphoprotein 32	2	0.50	1	1	-0.12	
C	P25490	YY1	Transcriptional repressor protein yy1	2	0.50	0	2	-0.13	
N	Q9H078	CLPB	Caseinolytic peptidase b	3	0.50	2	1	-0.14	
N	Q8WVC6	DCAKD	Dephospho-coa kinase domain containing	3	0.50	3	0	-0.15	
N	O75306	NDUFS2	Nadh dehydrogenase-ubiquinone fe-s protein 2	3	0.50	1	2	-0.15	
F	Q7L099	RUFY3	Protein rufy3	2	0.40	0	2	-0.16	
G	O15173	PGRC2	Membrane-associated progesterone receptor component 2	3	0.60	2	0	-0.16	
F	Q15165	PON2	Paraoxonase 2	2	0.40	2	0	-0.16	
C	Q9H4A5	GOLPH3L	Golgi phosphoprotein 3-like	2	0.50	2	0	-0.16	
M	Q9GZU8	FAM192A	Protein fam192a	3	0.75	2	1	-0.16	
M	A0A0C4DGV5Z	RANB2	Zis1	4	1.00	2	2	-0.20	
N	P10155	TROVE2	Ro ribonucleoprotein	4	0.67	3	1	-0.21	

M	Q7Z4V5	HDGFRP2	Hepatoma-derived growth factor-related protein 2	2	0.50	1	1	-0.22	
M	Q96JK2	DCAF5	Ddb1- and cul4-associated factor 5	2	0.50	0	2	-0.22	
C	Q9ULX6	AKAP8L	A-kinase anchor protein 8-like	2	0.50	1	1	-0.25	
M	Q96EY7	PTCD3	Pentatricopeptide repeat domain-containing protein 3	4	1.00	2	2	-0.25	
C	O95071	UBR5	E3 ubiquitin-protein ligase ubr5	2	0.50	0	2	-0.25	
N	Q8IWV7	UBR1	E3 ubiquitin-protein ligase ubr1	4	0.67	1	3	-0.26	
M	O00203	AP3B1	Ap-3 complex beta3a subunit	2	0.50	1	1	-0.29	42
M	O43164	PJA2	Praja ring finger 2	3	0.75	1	2	-0.30	
F	Q8IXB1	DNAJC10	Hypothetical protein	2	0.40	1	1	-0.32	
C	Q8TEB1	DCAF11	Gl014	3	0.75	2	1	-0.32	
C	O43933	PEX1	Peroxisome biogenesis factor 1	2	0.50	0	2	-0.36	
G	Q9NRX5	SERINC1	Kiaa1253 protein	2	0.40	2	0	-0.38	
N	Q96AC1	FERMT2	Mitogen inducible gene mig-2	3	0.50	0	3	-0.39	
C	Q13557	CAMK2D	Calcium/calmodulin-dependent protein kinase 2 delta	2	0.50	0	2	-0.39	
M	P30414	NKTR	Nk-tumor recognition protein	2	0.50	1	1	-0.50	
N	A0A024RCG7	ARMCX2	Armadillo repeat containing 6	3	0.50	2	1	-0.54	
N	I0B0K5	FLG	Truncated profilaggrin	2	0.33	1	1	-0.56	
M	P07199	CENPB	Cenp-b	2	0.50	0	2	-0.62	
N	Q5VYK3	ECM29	Proteasome-associated protein ecm29	2	0.33	1	1	-0.67	
F	Q5T5U3	ARHGAP21	Rho-gtpase activating protein 10	2	0.40	1	1	-0.94	
C	Q92621	NUP205	Nuclear pore complex protein nup205	3	0.75	2	1	-0.97	

a Indicates the number of replicates in which the protein was found

b Number of replicates in which the protein was found/ total number of replicates performed with the indicated bait

c Indicates the number of replicates in which the protein was found with the Nt or Ct TAP-tag

d Proteins sorted based on the Ave log (empai/med)

* PPI reported with other Nipah virus protein

** PPI reported with the equivalent Hendra virus protein

Table 2. List of drugs acting on potential Nipah virus therapeutic targets

Target	DrugBank ID	Drug group	Acts on
CAMK2D	DB06616	Approved	N
	DB08699	Experimental	
HLA-C	DB02740	Experimental	F
ALDH1L2	DB00116	Approved	F
ALDH3A2	DB00157	Nutraceutical	F
TFRC	DB05260	Approved	F
	DB06784	Approved	
	DB01592	Approved	
NDUS2	DB00157	Nutraceutical	N
	DB00997	Approved	
MTAP	DB00173	Approved	V
	DB02158	Experimental	
	DB02281	Experimental	
	DB02282	Experimental	
	DB02933	Experimental	

Table 3. GO (Biological Process) of differentially expressed genes

Gene Set Name	# Genes	# Genes in overlap	q-value
DNA Packing	194	17	9.58 e-21
Chromatin organization	663	21	3.42 e-17
Chromatin silencing	95	9	9.29 e-11
Innate Immune response in mucosa	23	6	1.31 e-9
Defense response	1231	18	3.87 e-9

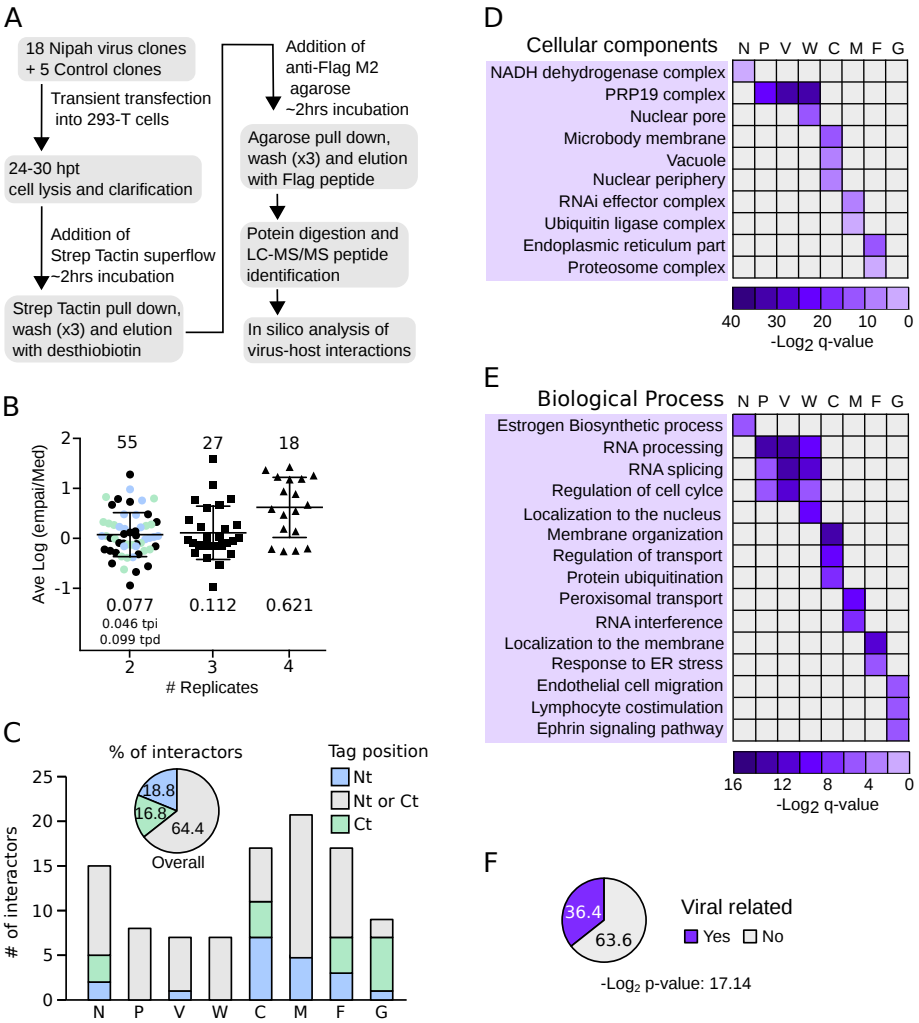

Figure 1

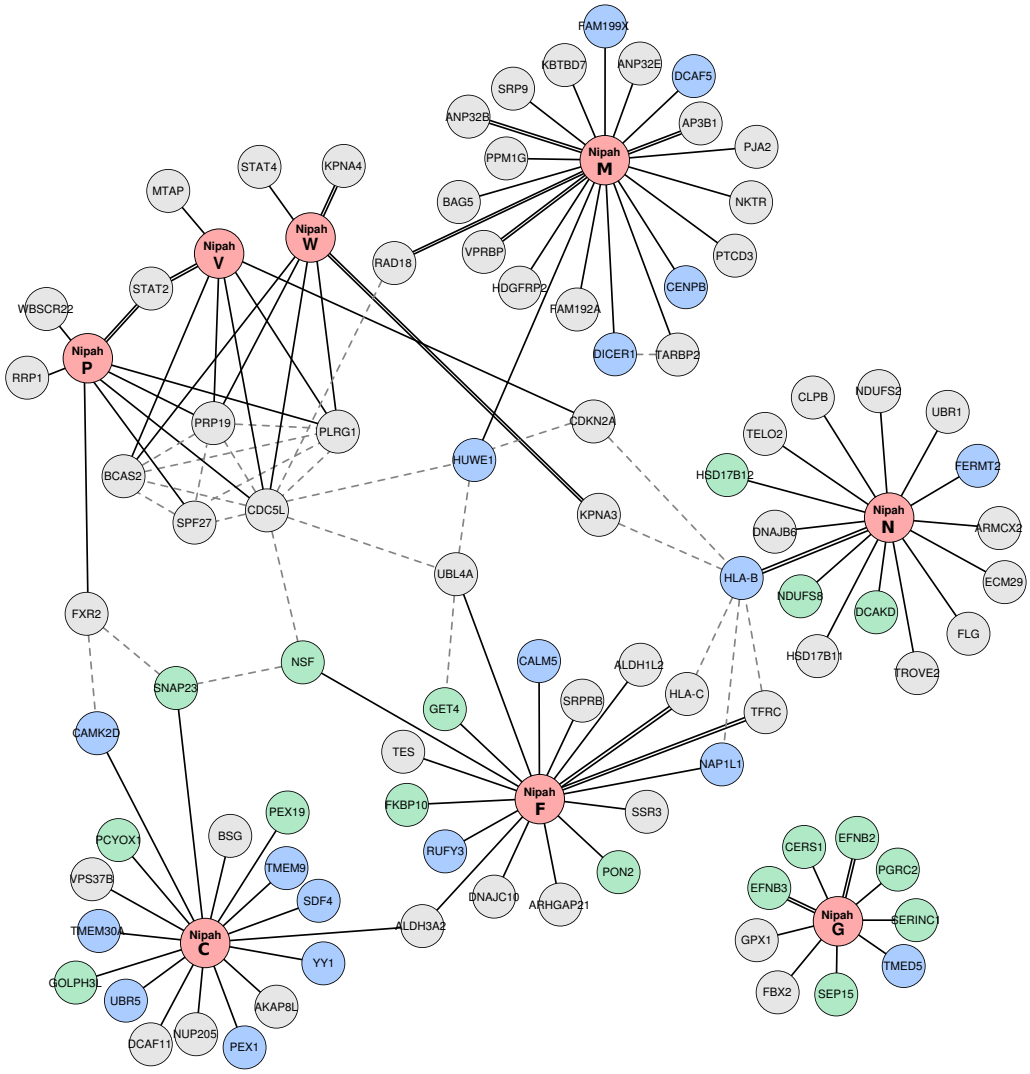

Figure 2

Figure 3

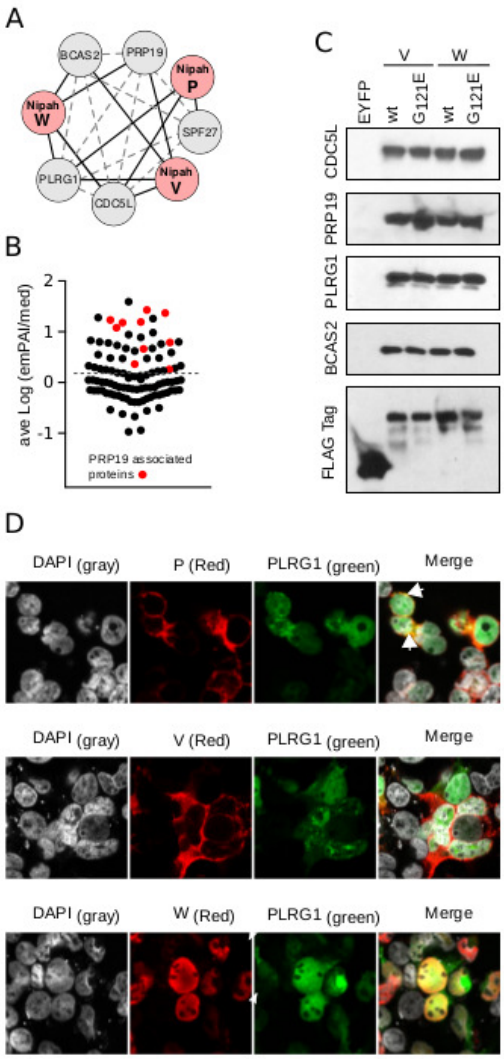

Figure 4

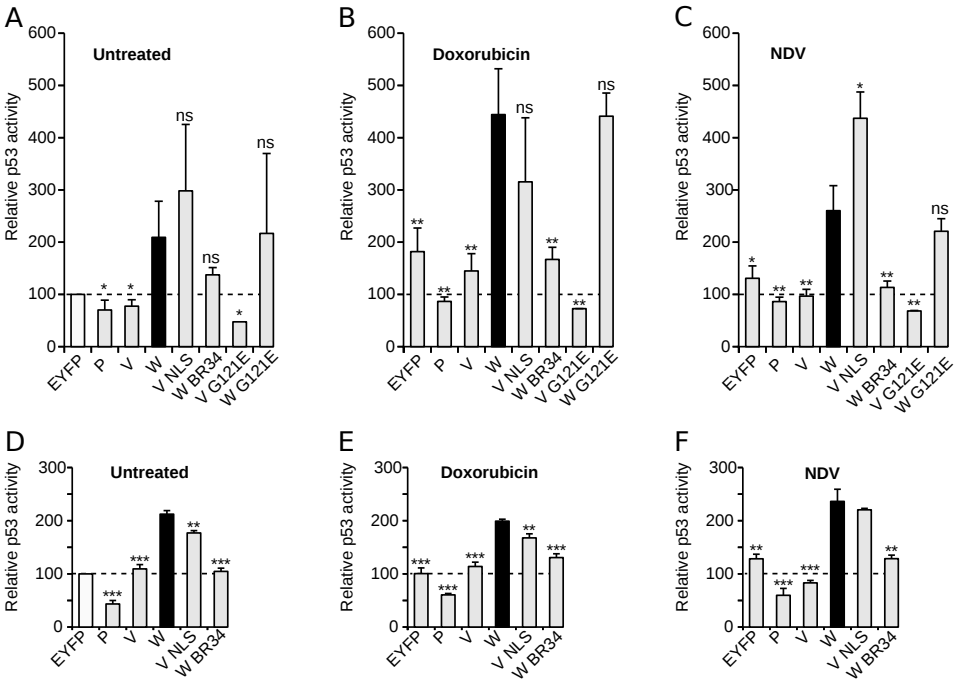

Figure 5

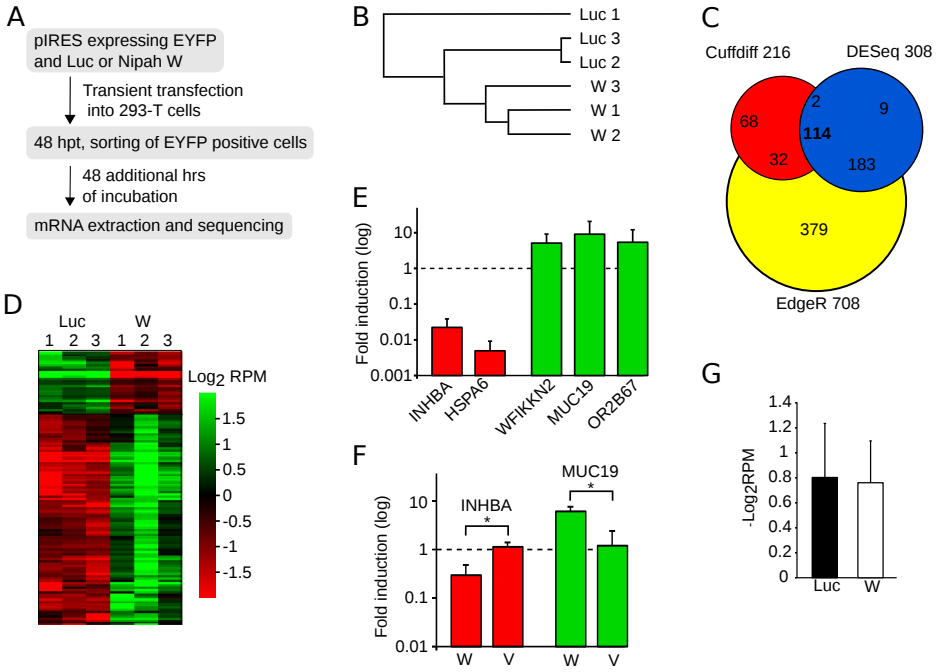

Figure 6

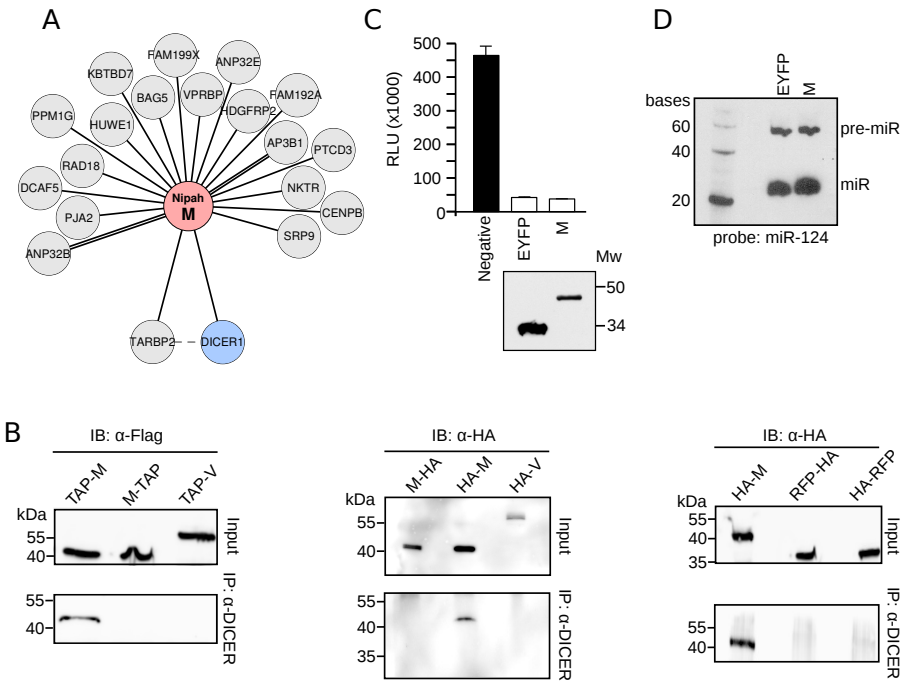

Figure 7